Structural and compositional changes during mechanical milling of the Fe–Cr system

2005 J. Phys.: Condens. Matter 17 7981

(http://iopscience.iop.org/0953-8984/17/50/016)

INSTITUTE OF PHYSICS PUBLISHING JOURNAL OF PHYSICS: CONDENSED MATTER

J. Phys.: Condens. Matter **17** (2005) 7981–7993 doi:10.1088/0953-8984/17/50/016

Structural and compositional changes during mechanical milling of the Fe–Cr system

Brajesh Pandey[1], **M Ananda Rao**[2], **H C Verma**[1,3] **and S Bhargava**[2]

[1] Department of Physics, Indian Institute of Technology, Kanpur 208 016, India
[2] Department of MME, Indian Institute of Technology, Kanpur 208 016, India

E-mail: hcverma@iitk.ac.in

Received 25 June 2005, in final form 24 October 2005
Published 2 December 2005
Online at stacks.iop.org/JPhysCM/17/7981

Abstract

The structural and compositional changes during mechanical milling of Fe–Cr powder (10 wt% Cr) were followed by scanning electron microscopy (SEM), atomic force microscopy (AFM), x-ray diffraction (XRD), Mössbauer spectroscopy and magnetization measurement. All these techniques give complementary information about the alloying process during milling. Different particles are cold welded and elongated to form composite granules in the initial stage of milling (5–10 h). The crystalline order is also destroyed heavily and nanosize crystallites are formed during early milling. Chromium diffusion in the iron lattice starts somewhat late (after 20 h of milling) when composite granules flatten, reducing the distance between iron and chromium layers. Though compositional homogeneity is achieved up to nanometre scale in 65 h of milling, atomic diffusion of the species still continues up to 100 h of milling.

1. Introduction

Mechanical alloying of elemental metallic powders is now developed as an effective tool to produce a wide variety of equilibrium and non-equilibrium phases. The mechanism of alloying during the mechanical milling process has been studied in great detail [1–6]. In essence, the inter-dispersion of alloying elements occurs due to repeated cold welding and fracture of free powder particles arising from the impact energy of milling medium in a high energy attrition mill. Such a cold welding results in layers of powder particles joining together to form composite granules. The heavily dislocated structure formed due to the large scale deformation of individual particles or of the granules during their cold welding enhances the mutual solubility of elements and leads to their mixing at the atomic scale by progressively eliminating the concentration gradient in the composite granules. Therefore, mechanical alloying is capable

[3] Author to whom any correspondence should be addressed.

of producing powders in a non-equilibrium state by either accumulating mechanical energy or accelerating diffusion across the interface between unlike elements [7–13]. The grain size of the alloyed material also simultaneously decreases as a function of milling time and eventually reaches a nano-scale. In some cases the continuous milling of the powder may also lead to the formation of amorphous phase [1–5, 14]. The formation of alloy from milling, however, depends on many parameters such as milling conditions and thermodynamic properties of the milled system.

Starting from elemental powders, several workers have used the mechanical alloying approach for producing Fe–Cr alloys of different compositions [15–17]. These studies show that mechanical alloying is indeed capable of producing a nanoscale structure with grain size of ∼10 nm [17, 18]. The progress of alloying in mechanically alloyed powders as well as refinement of grain size during the course of milling can generally be inferred from x-ray diffraction. However, the compositional heterogeneity such as the fraction of Cr mixed with Fe cannot be inferred from XRD because the diffraction peaks of Cr and Fe overlap. In contrast, due to different magnetic properties of Fe and Cr and a strong compositional dependence of magnetic properties in the Fe–Cr system, Mössbauer spectroscopy can be used to find the compositional heterogeneity in the alloys synthesized and thus the progress of mechanical alloying can be followed. Mössbauer spectroscopy has thus been used by several workers [15, 19, 20] to study mechanically alloyed systems. In addition, SEM and AFM are imaging techniques suited to morphological studies such as dependence of grain shape on milling time, and of lamellar spacing in the composite granules on milling time. While SEM gives information at the micron scale and AFM gives information at the nanometre scale, Mössbauer spectroscopy gives information at the atomic scale in the immediate surroundings of ^{57}Fe atoms. In the present article, SEM, AFM, XRD and Mössbauer spectroscopic studies of Fe–Cr alloys produced by mechanical alloying are presented. The kinds of information from the above techniques are complementary to each other and collectively they reveal the changes at various levels as the milling progresses.

2. Experimental procedures

Iron and chromium powders of purity greater than 99.99% were used for the purpose of mechanical alloying. Powders had been sealed and stored in the argon glove box to ensure no oxygen contamination during their storage. Fe and Cr powders corresponding to Fe–10 wt% Cr were separately weighed in the argon glove box itself. This corresponds to the composition Fe 89.3 at.% Cr 10.7 at.%. The milling batch had a mass of 50–55 g. Weighed powders, along with grinding media steel balls, were transferred in the steel jars within the argon glove box itself. The milling charge could thus be maintained under the argon atmosphere. The charge to ball ratio for each milling operation was maintained as 1:8.

Powder milling was carried out in a Retsch type planetary ball mill. The milling speed was kept at 250 rpm and the size of the balls taken was 10 mm. For the purpose of monitoring the nature of milling and alloying, the milling operation was intermittently stopped after milling times of 5, 10, 15, 20, 40, 65 and 100 h. After each such operation milling jars were transferred to the argon glove box and small amounts of powder samples (roughly 1–1.5 g) were taken out for the purpose of characterization.

Powder samples taken out of the planetary ball mill after different time intervals were characterized using the x-ray diffraction technique. The instrument used was a Seifert Iso-Debyflex 2002 diffractometer with copper target. The tube was operated at 30 kV and 10 mA. The radiation used was Cu Kα having a wavelength of 0.154 nm. The scanning rate in the x-ray powder diffraction was kept at 3° min^{-1}. The peak broadening was used

to estimate the crystallite (grain) size. In order to remove the effect of broadening due to instrumental interference, the XRD pattern of highly crystalline silicon was recorded in the same experimental conditions as used with the milled powder samples. The FWHM obtained after removal of the instrumental broadening effect was input to Scherrer's equation to determine crystalline size.

Powder morphology of mechanically alloyed samples was analysed under a JEOL JSM 840A scanning electron microscope. The milled powder morphologies were observed by dispersing the powders with acetone on finely polished brass stubs prepared especially for this purpose. The samples were also imaged with atomic force microscopy (Molecular Imaging, USA), operated in acoustic AC mode (AAC) with the aid of a cantilever (NSC 12 (c) from MikroMasch). The force constant was 2.4 N m^{-1}, while the resonant frequency was 150 kHz. The images were taken in air at room temperature, with the scan speed of 1.5–2.2 lines s^{-1}. Data acquisition was done by using PicoScan5 software, while the data analysis was done with the aid of visual SPM. The Fe–Cr mechanically alloyed powders of different milling times were sprinkled over a freshly cleaved mica surface, and uniformly spread with the aid of a spin-coater. Then mica was dried for 30 min, at room temperature, followed immediately by imaging with AFM.

For Mössbauer spectroscopy, samples were sandwiched between two layers of Sellotape in a copper ring of 13 mm inner diameter. The data were recorded at room temperature in a transmission geometry using a conventional ^{57}Fe constant acceleration Mössbauer spectrometer employing a 25 mCi ^{57}Co/Rh source. The spectra were analysed using the least squares method assuming Lorentzian lineshapes. Magnetization measurements were made using a vibrating sample magnetometer (VSM).

3. Results and discussions

3.1. Particle morphology

Some representative scanning electron micrographs of the milled powders are shown in figure 1. The morphology of the 5 h milled sample shows different particles sticking over one another and cold welded to form composite granules. The size of these granules is several tens of micrometres and in fact it increases initially with milling because of impact welding of particles. As the powder is milled for 20–40 h, these granules become elongated, and work hardened and therefore they fracture. The shape of these granules changes drastically between 40 and 65 h of milling. For both 65 and 100 h of milling, the granules are very flat and flaky. As the flattened granules become work hardened they resist further impact welding and the impact results only in further flattening and fracture.

3.2. Phase contrast study in AFM

The phase data in tapping mode AFM results from the phase lag between the AC drive input and the cantilever oscillation output at each probe location. Consequently, contrast in phase images arises due to differences in material properties such as chemical heterogeneity and the associated defects, elastic moduli, adhesion, friction, viscoelasticity etc. In view of the fact that both Fe and Cr have very similar atomic radii, and both crystallize in the BCC structure with very similar lattice parameters, the main contribution to the phase contrast in AFM images from milled Cr–Fe powders is likely to come from the compositional heterogeneity in Fe–Cr solid solutions and defects associated in its structure.

Phase contrast images from the powders of Fe–Cr after different milling times are shown in figure 2. The image of the powder milled for 20 h shows regions of dark phase in a brighter

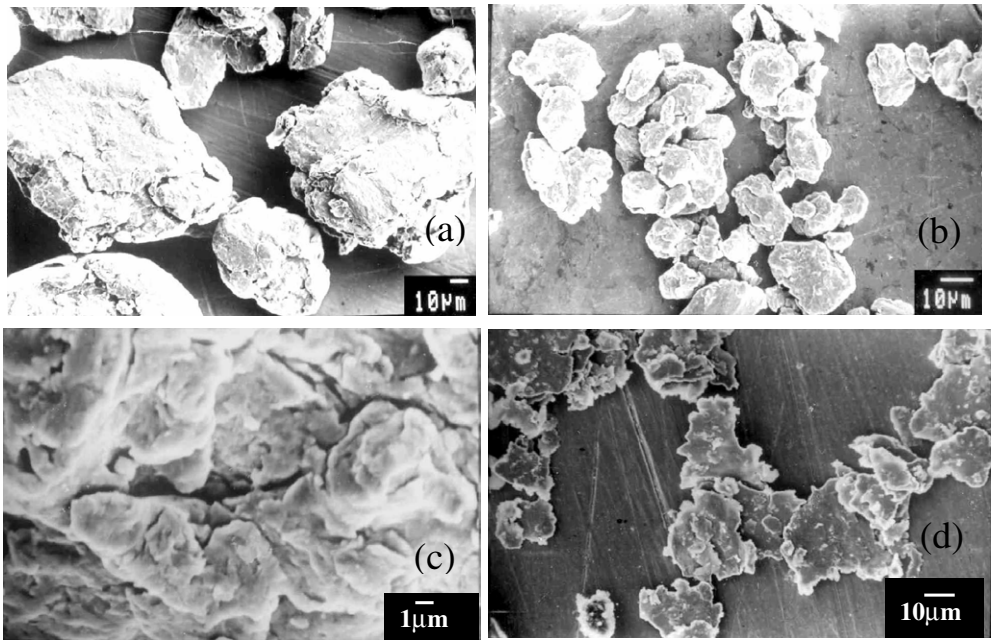

Figure 1. SEM micrographs of ball milled samples. (a) 5 h, (b) 20 h, (c) 40 h and (d) 100 h.

matrix. Most likely the two shades correspond to two different compositions of the Fe–Cr system. The image shows a large inhomogeneity at the nanometre scale. As the milling time increases the length scale of the inhomogeneity between dark and bright phases reduces. While the compositional heterogeneity in the structure (represented as dark and white phases) in the powder milled for 20 h varies in the size range of ∼15 to ∼120 nm, that in the powder milled for 40 h varies in the size range of ∼5 to ∼60 nm. The images from powders milled for 65 and 100 h do not show such features and instead show a more or less dimpled type of structure. It may be assumed that the regions of compositional heterogeneity become finer than 5 nm scale for a milling time between 40 and 65 h and ultimately disappear, giving rise to a compositionally homogeneous solid solution of Fe–Cr. The dimple structures in the phase contrast images of 65 and 100 h have a length scale of a few nanometres. The regular structure shows that 65 h milling results in compositional uniformity at the nanometre scale.

3.3. X-ray diffraction

The XRD patterns of all the powder samples are shown in figure 3. Both the constituents, Fe and Cr, crystallize in the body-centred cubic (BCC) structure and the difference in their lattice parameters is only 0.5%. Thus the diffraction peaks from Cr and Fe overlap strongly, making it very difficult to follow the progress of mechanical alloying in terms of decrease in peak intensities of the original constituents and formation of new peaks. However, XRD patterns could be used for determination of crystallite size. The crystallite size of milled Fe–Cr powders and its reduction with milling time was monitored by analysing the FWHM of the most intense peak and using Scherrer's formula.

As the peak positions of Fe and Cr are close to each other (44.94° for Fe and 44.58° for the Cr 110 peak), they strongly overlap in an Fe–Cr system. To look for the peak broadening due to this overlap, we recorded the XRD of a 90% Fe, 10% Cr mixture and analysed the

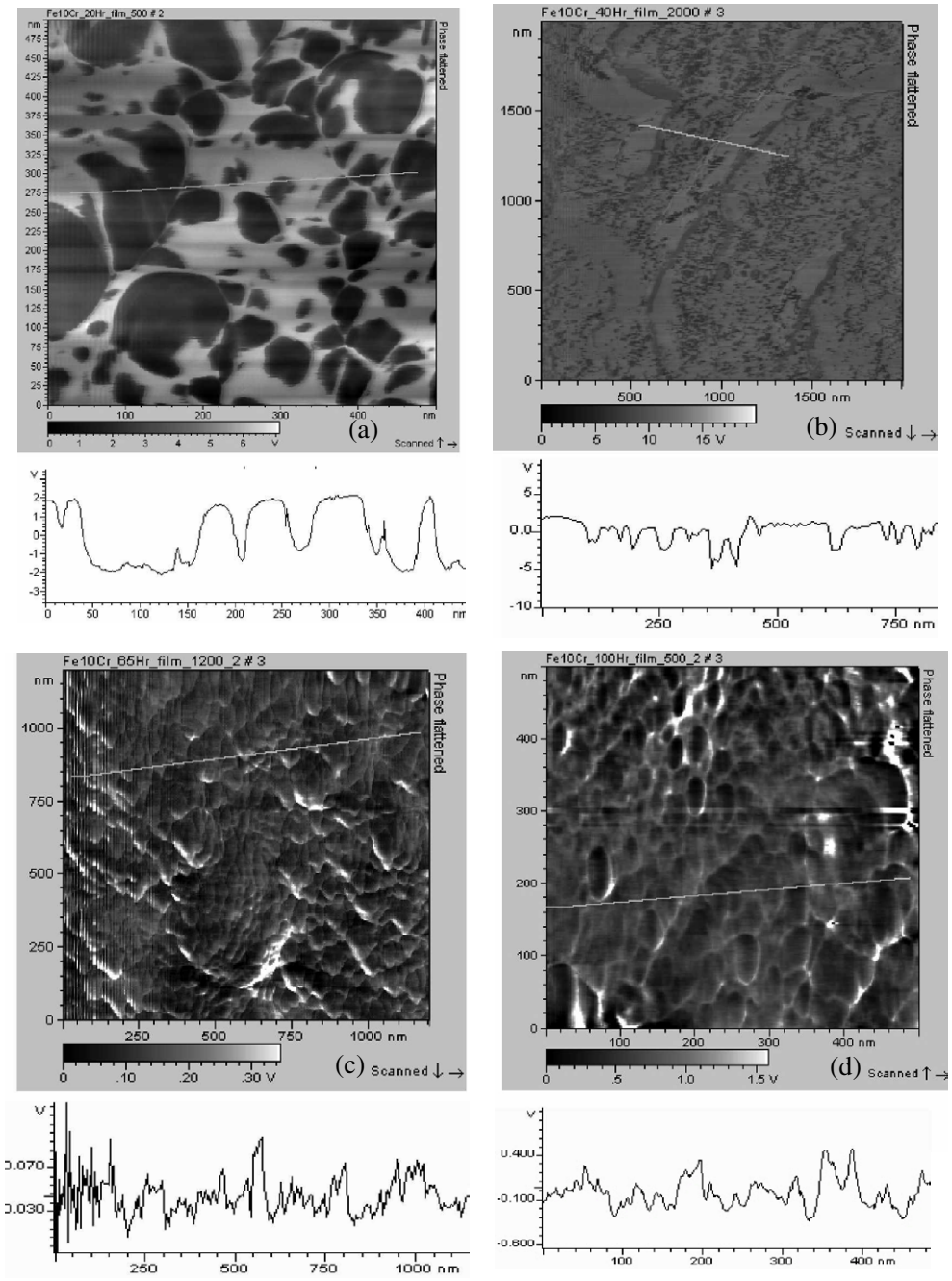

Figure 2. AFM phase contrast images of ball milled samples. (a) 20 h, (b) 40 h, (c) 65 h and (d) 100 h.

pattern for the FWHM of the 110 peak. While pure iron gave a crystallite size of 77 nm, the crystallite size deduced from the XRD of the mixture was 71 nm. Thus the effect of overlap of peaks was only nominal (less than 8%) and we assume that any further broadening due to milling reflects the reduction in the crystallite size.

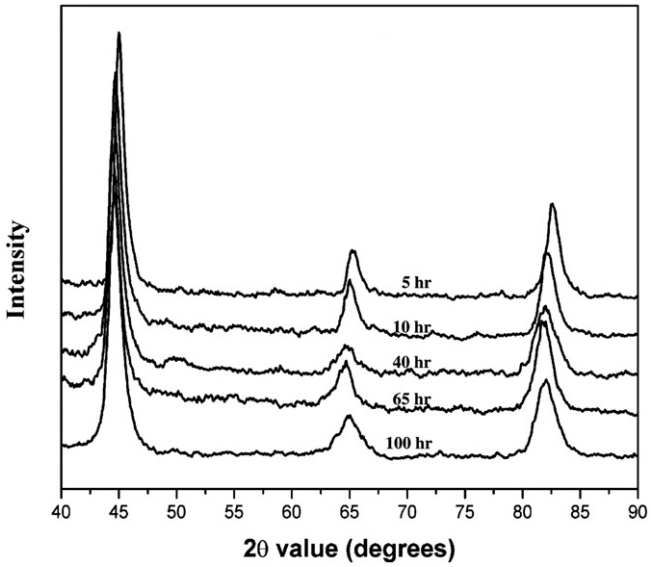

Figure 3. XRD patterns of the Fe–Cr powder milled for different periods.

The effect of milling time on the crystallite size of Fe–Cr powder is shown in figure 4. The error bars are obtained from the estimate of error (∼0.02°) in the measurement of FWHM. It can be seen that crystallites of size as small as 10 nm are formed in the first 10 h. Subsequently the rate of decrease of crystallite size was found to be less rapid. Beyond the milling time of 40 h, the crystallite size was found to be almost constant at 7 nm. As shown by SEM studies, the powder particles are deformed severely due to impact in the initial phase of milling, which causes accumulation of defects, dislocations, stacking faults, etc., and these features cause severe distortions in the lattice. These defects become localized in the shear bands formed and then disintegrate into small grains (crystallites) due to higher instability of the structure [11]. Thus rapid decrease in crystallite size is the first observable effect of milling.

It can be seen that the peak positions shift towards lower values as the milling time increases. This trend continues till 40 h of milling, after which there is no observable peak shift. The decrease in the 2θ values of the peaks indicates increase in the lattice parameter, which may occur due to the reduction of crystallite size. Such a lattice expansion in nanocrystalline material has been observed for several systems and is attributed to the interface structure which has a large volume fraction for nanosize samples [21, 22]. After 40 h of milling time the crystallite size remains almost the same (figure 4) and the XRD peaks also do not show any shift, supporting the assumption that the lattice expansion is due to crystallite size reduction.

The lattice parameter of Fe–Cr alloy is known to increase with Cr concentration [19]. It may be tempting to interpret the increase in lattice parameter with milling time as due to greater fraction of alloying. However, Mössbauer studies, described in the next section, rule out this possibility.

3.4. Mössbauer spectroscopy

While SEM shows particle morphology usually at the micron scale and AFM phase contrast study tells about heterogeneity (atomic number, adhesion, etc) at the nanometre scale, Mössbauer spectroscopy gives information about the surroundings of Fe atoms at the

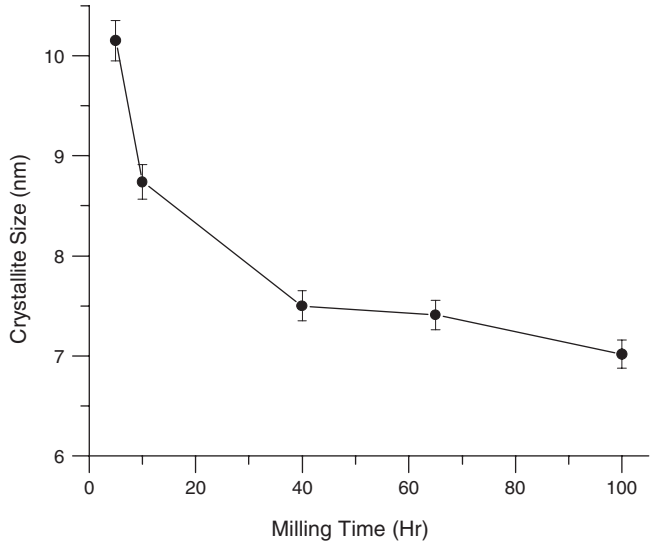

Figure 4. Crystallite size estimated from XRD pattern as a function of milling time.

atomic scale. It can therefore address questions like whether Cr is diffusing in the Fe crystal or Fe is diffusing in the Cr crystal, or what is the composition in the nearest neighbour and the next nearest neighbour cells of the Fe atoms.

Figure 5 shows the Mössbauer spectra of milled Fe–Cr powders. Each of the spectra of samples milled up to 20 h consists of a single six-line pattern characteristic of the pure iron phase. This means that up to 20 h there is almost no interdiffusion of Cr and Fe into each other's crystal. While XRD patterns show sharp decrease in the crystallite size, SEM shows sharp changes in the granular morphology, AFM shows heterogeneous composition of Fe and Cr, Mössbauer spectra clearly show no interdiffusion of Fe and Cr up to 20 h of milling.

There is a drastic change in the shape of the spectrum as the milling time is increased to 40 h. A number of other six-line patterns appear, showing that chromium has started entering the Fe matrix on milling between 20 and 40 h. At this stage the SEM micrograph (figure 2(c)) shows lot more elongation and flattening of the welded granules. The flattened structure of the composite granules could increase the surface area for diffusion and also reduce the thickness of layers of Fe and Cr in the granules. Both these would help in atomic diffusion. The reduced contrast in AFM (figure 2(b)) also supports that interdiffusion has started. The shape of the Mössbauer spectrum does not change much as the milling time is increased to 65 h. The SEM micrographs show that by this time the granules have acquired flaky structure. However, the conversion to complete flaky structure has not changed the environments of iron considerably as at least visually the Mössbauer spectra of 40 and 65 h milled samples do not show much change.

Interestingly, the SEM and AFM pictures of 65 and 100 h samples do not show much change, as if alloying is complete by 65 h and homogeneity has been achieved. Similarly, the crystallite size and the lattice parameter also seem to stabilize by 65 h of milling. But the Mössbauer spectrum of the 100 h sample does differ from that of the 65 h sample, showing that the alloying is definitely not complete in 65 h at the atomic level. Attaining homogeneity in morphology, crystal structure etc does not ensure compositional homogeneity at the atomic level and more milling is needed after obtaining the structural homogeneity to get full alloying.

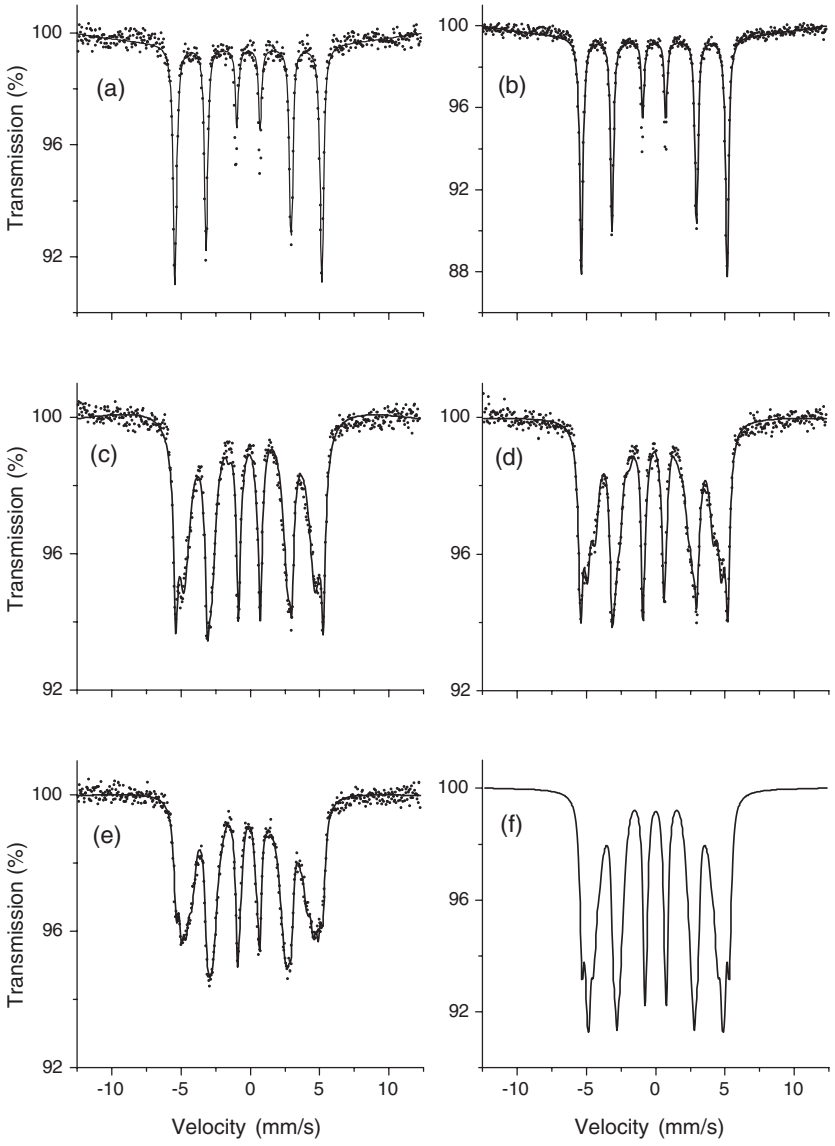

Figure 5. Mössbauer spectra of Fe–Cr powder milled for different periods. The solid line represents the least squares fitted lineshape assuming it to be a superposition of Lorentzian functions. (a) 5 h, (b) 20 h, (c) 40 h, (d) 65 h and (e) 100 h ball milled sample; (f) simulated spectrum of ideal solid solution with composition $Fe_{90}Cr_{10}$.

The above discussion is based on the qualitative visual appearance of the Mössbauer spectra. To get more quantitative information we have analysed all the Mössbauer data in terms of a continuous variation of hyperfine magnetic field (HMF) B_{hf}. The probabilities for different values of B were calculated using the Caer and Dubois approach [23]. The p–B distributions for different samples are shown in figure 6.

The HMF in pure iron samples is 33.0 T. Each chromium atom substitution in the nearest neighbour (nn) cell reduces the HMF by about 3.0 T and each chromium atom substitution

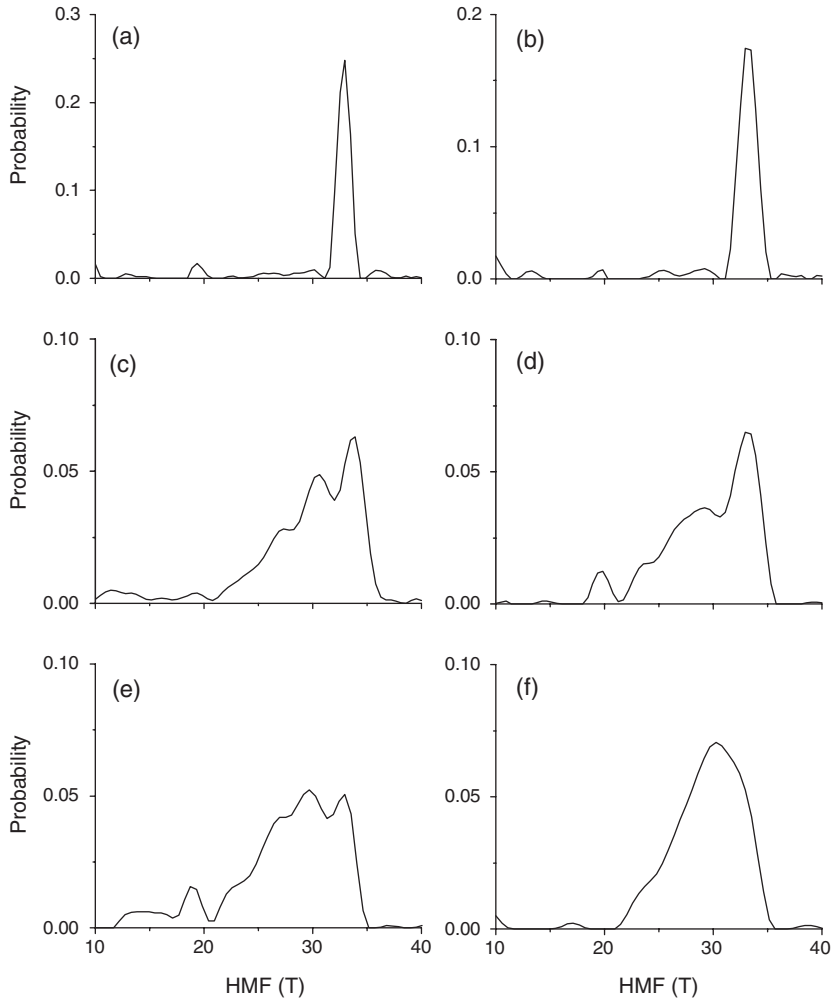

Figure 6. p–B distributions of Fe–Cr powder milled for different periods. (a) 5 h, (b) 20 h, (c) 40 h, (d) 65 h and (e) 100 h ball milled samples; (f) p–B distribution from the simulated spectrum of the ideal solid solution with composition $Fe_{90}Cr_{10}$.

in the next nearest neighbour (nnn) cell reduces the HMF by 2.0 T [20]. For a completely alloyed solid solution, the numbers of chromium atoms in the nn and nnn cells are distributed according to the binomial distribution [24]

$$P(m, n, q) = {}^{8}C_m \, {}^{6}C_n q^{m+n}(1-q)^{14-m-n} \tag{1}$$

where q is the atomic fraction of chromium atoms and m and n are the numbers of chromium atoms in nn and nnn cells respectively. Using this we have simulated the ideal Mössbauer spectrum for the completely alloyed Fe–Cr system of our composition. The p–B distribution fitted to this simulated spectrum is shown in figure 6(f).

As expected, the fitted p–B distributions for samples up to 20 h of milling time show only a single peak at 33.0 T corresponding to no diffusion of chromium in the Fe matrix, that means $m = 0$ and $n = 0$. The p–B distributions of 40, 65 and 100 h samples show multipeak structures showing that some of the other possible m, n environments are growing. To further

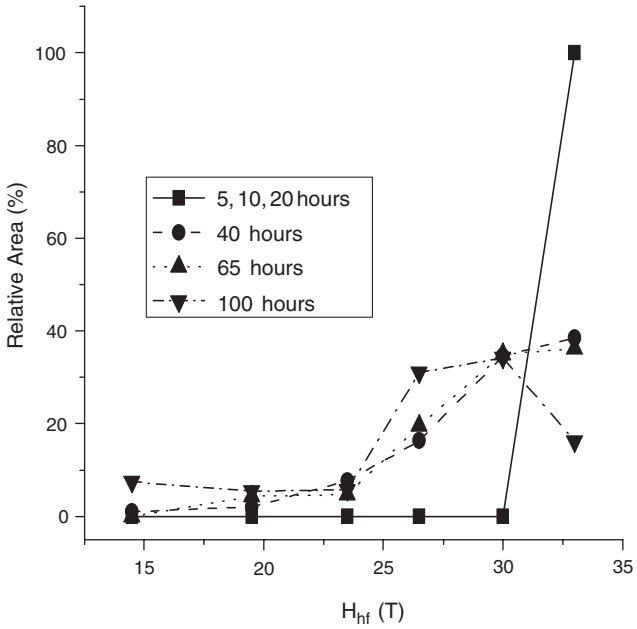

Figure 7. Relative areas in the p–B distributions corresponding to different B_{hf} groups.

study the differences in the p–B distributions, we have fitted a set of six Gaussians to each of the p–B distributions. The results are shown in figure 7. The Gaussians are centred roughly around 33.0, 30.0, 26.5, 23.5, 19.5 and 14.5 T. The first of these corresponds to no chromium diffusion in the nn and nnn cells of iron and others correspond to gradually more chromium atoms diffusing in the Fe environment. We see that for 5, 10 and 20 h milled samples only the 33.0 T component exists, corresponding to the fact that despite structural changes such as impact welding and fracturing no significant mixing has occurred at the atomic level. A lot of alloying has taken place between 20 and 40 h, where the relative area under the 33.0 T Gaussian is reduced drastically (from 100% to about 39%) and all the other environments have grown, the largest gainer being 30.0 T. From 40 to 65 h, there is no significant change in the areas of the Gaussians fitted. Significantly, between 65 and 100 h, there is considerable reduction in the area of the Gaussian under 33.0 T, where it drops from about 36% to 20%. This shows that large numbers of Cr atoms are diffusing in the iron lattice during this period. As a Cr atom goes in the nn or nnn cell of Fe, where there was no Cr to start with, the contribution of 33.0 T decreases. This should be accompanied by an increase in the contribution of the Gaussian at 30.0 T. But Cr is also getting into the cells of Fe which already had one Cr atom, and this keeps the area of the 30.0 T Gaussian almost the same. The contribution from the 26.5 T Gaussian increases, corresponding to diffusion of Cr atoms in the cells where already a Cr atom was present. So once the flakes are formed (after 65 h), the chromium diffusion has enhanced and alloying is further facilitated.

An estimate of the fraction of Cr alloyed as a function of milling time can be had from the nature of the p–B distribution. From figure 7 we see that the contribution of 33.0 T B_{hf} reduces from 100% to about 39% between the milling of 20 to 40 h and remains almost the same up to 65 h of milling. We have calculated from equation (1) that q should be 0.06 to result in the contribution of zero Cr in nn and nnn cells to be about 39%. Though the situation is complicated by presence of various kinds of defects and nonequilibrium composition during

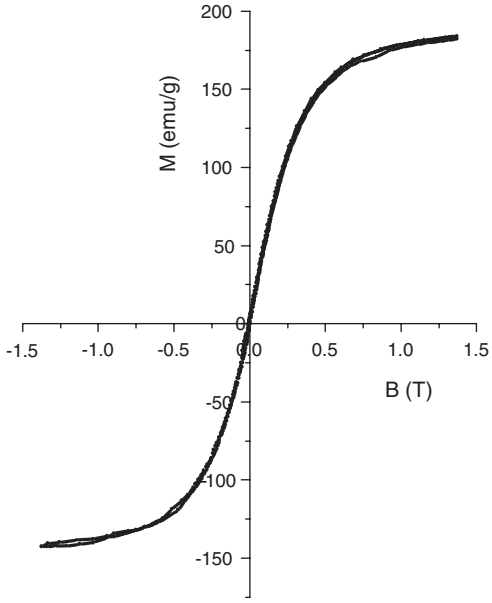

Figure 8. Typical curve of magnetization (M) versus applied magnetic field (B) for 5 h milled Fe–Cr powder.

the ongoing alloying process, we can give a rough estimate that in 40 h of milling about 6% of Cr has gone into the iron lattice. With $q = 0.10$, equation (1) tells that the contribution of zero Cr in nn and nnn cells of the Fe should be 22%. The observed area of 20% under the 33.0 T Gaussian for 100 h milled samples shows that almost all the Cr has gone into the Fe lattice at this stage.

However, even the p–B distribution for the 100 h milled sample is not very close to the simulated p–B distribution (figure 6(f)). Although almost all the chromium has entered the Fe lattice, compositional homogeneity in the solid solution is yet to be achieved.

3.4.1. Preferential diffusion of chromium atoms. Both Fe and Cr particles must have participated in forming composite granules which undergo various structural changes like flattening and achieving flaky structure. During the milling chromium atoms have diffused into Fe matrix much more readily (to give B_{hf} smaller than 33.0 T) than the iron atoms in the Cr matrix. If iron atoms diffused into the Cr matrix they would find Cr atoms throughout the neighbourhood and would give a singlet [15–17, 19, 25]. No such component was detected in any of the Mössbauer spectra, showing that chromium diffusion in the iron matrix is preferred over iron diffusion in the chromium matrix.

3.5. Magnetization measurement

The magnetization of the milled samples was measured with an applied field up to 1.37 T for a full cycle of increasing and decreasing field to get the saturation magnetization and the hysteresis. All samples show M–B curves typical of a ferromagnetic system with a small coercive field. Figure 8 shows a representative M–B curve of the 5 h milled sample. The values of saturation magnetization of the samples milled for various numbers of hours are shown in figure 9.

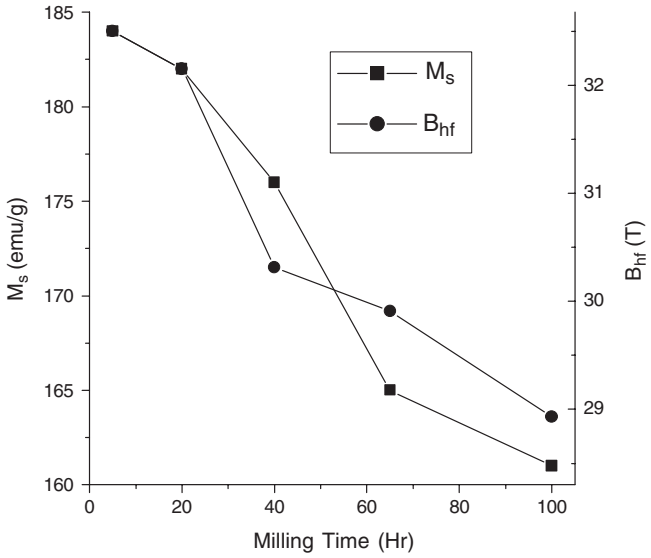

Figure 9. The variation of saturation magnetization (M_s) (solid squares) and average hyperfine magnetic field (B_{hf}) (solid circles) with milling time.

We see that the saturation magnetization decreases slightly up to 20 h of milling and then decreases sharply as the milling time is increased to 40 h. It supports the conclusion from Mössbauer spectroscopy that up to 20 h of milling no significant diffusion of Cr in Fe takes place. If we assume that the magnetization is reduced from that of the pure iron according to the law of dilution, we would expect a value of 198 emu g^{-1} for saturation magnetization. The observed value of 184 emu g^{-1} for the 5 h milled sample and 182 emu g^{-1} for the 20 h milled sample is somewhat smaller than this. This reduction might come from the rupturing of crystalline structure during milling, which reduces the crystallite size into the nanometre range even in 5 h milling. The magnetic domains are also likely to get reduced in size, reducing the average magnetization. As the sample is milled further, Cr enters the lattice of Fe and forms alloy. It is known that Cr inclusion in the iron lattice reduces the magnetization, due to reduced coupling strength between Fe and Cr magnetic moments [26]. This trend of decreasing saturation magnetization continues even up to 100 h of milling, showing that alloying is still going on. This again confirms that although the crystallite size, particle morphology and compositional homogeneity at the nanometre scale are the same for 65 and 100 h of milling, the picture at the atomic scale is different. Figure 9 also shows the average hyperfine magnetic field B_{hf} for the samples. This is calculated from the p–B distribution shown in figure 6. We see a nice correlation between the saturation magnetization M_s and the hyperfine magnetic field B_{hf}, showing that the alloying proceeds as proposed.

4. Conclusion

The processes taking place during mechanical milling of Fe, Cr powders have been studied in detail by obtaining the complementary information through SEM, AFM, XRD, Mössbauer spectroscopy and magnetization measurement. The whole sequence can be divided into four phases. In the initial phase the particles get impact welded, because of which the granule size grows. At the same time because of the impacts the regular crystalline structure is altered,

leading to formation of crystallites of size up to 10 nm. No mixing of two kinds of atoms in each other's matrix takes place up to 20 h of milling in our case. Also, Fe-rich and Cr-rich regions separately exist with length scale of more than 100 nm. Then comes the second phase, in which a lot of flattening and fracturing takes place and chromium atoms diffuse in the iron matrix at a quite high rate. Though both chromium and iron lattices are deformed, only chromium atoms diffuse in iron matrix and not *vice versa*. The compositional heterogeneity is reduced to a few nanometres. The third phase can be identified during 40–65 h of milling, where the fractured particles are broken into smaller pieces and highly flattened due to impacts of balls. This induces severe structural deformation, and chromium atoms enter Fe cells and produce more environments where one or two chromium atoms are present in the neighbourhood of an iron atom. However, the overall crystallite size becomes quite uniform in this phase and the compositional heterogeneity reduces to a few nanometres. This means that at nanometre resolution Cr and Fe seem to have made a solid solution. But the same is not true at the angstrom scale. Once the flaky structure is attained, further milling (65–100 h), which may be termed as the fourth phase, facilitates chromium diffusion in the direction of producing a solid solution of Cr and Fe without any significant change in either the grain size or particle morphology. However, the solid solution state at the atomic level is not completed even after 100 h of ball milling.

References

[1] Koch C C 1991 Processing of metals and alloys *Materials Science and Technology—A Comprehensive Treatment* vol 15, ed R W Cahn (Weinheim: VCH) p 193
[2] Suryanarayana C 1995 *Bibliography on Mechanical Alloying and Milling* (Cambridge: Cambridge International Science Publishing)
[3] Suryanarayana C 1996 *Met. Mater.* **2** 195
[4] Lai M O and Lu L 1998 *Mechanical Alloying* (Boston, MA: Kluwer–Academic)
[5] Murty B S and Ranganathan S 1998 *Int. Mater. Rev.* **43** 101
[6] Suryanarayana C 2001 *Prog. Mater. Sci.* **46** 1
[7] Turnbull D 1981 *Metal. Trans.* A **12** 695
[8] Shingu P H 1993 *Processing Materials for Properties* ed H Henein and T Oki (Warrendale, PA: TMS) p 1275
[9] Froes F H, Suryanarayana C, Russell K and Ward-Close C M 1994 *Novel Techniques in Synthesis and Processing of Advanced Materials* ed J Singh and S M Copley (Warrendale, PA: TMS) p 1
[10] Froes F H, Suryanarayana C, Russell K and Li C-G 1995 *Mater. Sci. Eng.* A **192/193** 612
[11] Suryanarayana C (ed) 1999 *Non-Equilibrium Processing of Materials* (Oxford: Pergamon)
[12] Liebermann H H (ed) 1993 *Rapidly Solidi Alloys: Processes, Structures, Properties, Applications* (New York: Dekker)
[13] Anantharaman T R and Suryanarayana C 1987 *Rapidly Solid Metals—A Technological Overview* (Aedermannsdorf: Trans Tech Publications)
[14] Ermakov A E, Yurchikov E E and Barinov V A 1981 *Phys. Met. Metallogr.* **52** 50
[15] Koyano T, Takizawa T, Fukunaga T, Mizutani U, Kamizuru S, Kita E and Tasaki A 1993 *J. Appl. Phys.* **73** 429
[16] Lemoine C, Fnidiki A, Lemarchand D and Tellet J 1999 *J. Magn. Magn. Mater.* **203** 184
[17] Murugesan M and Kuwano H 1999 *IEEE Trans. Magn.* **35** 3499
[18] Lemoine C, Fnidiki A, Lemarchand D and Tellet J 1999 *J. Phys.: Condens. Matter* **11** 8341
[19] Petrov Yu I, Shafranovsky E A, Krupyanskii Yu F and Essine S V 2002 *J. Appl. Phys.* **91** 352
[20] Dubiel S M and Zukrowski J 1981 *J. Magn. Magn. Mater.* **23** 214
[21] Dias A, Moreira R L, Mohallem N D S and Persiano A I 1997 *J. Magn. Magn. Mater.* **172** L9
[22] Wang L and Li F S 2001 *J. Magn. Magn. Mater.* **223** 233
[23] Caer G Le and Dubois J M 1979 *J. Phys. E: Sci. Instrum.* **12** 1083
[24] Wertheim G K, Jaccarino V, Wernick J H and Buchanan D N E 1964 *Phys. Rev. Lett.* **12** 24
[25] Cieślak J, Dubiel S M and Sepiol B 2000 *J. Phys.: Condens. Matter* **12** 6709
[26] Pandey B and Verma H C 2005 *Pramana* **64** 281